Available online at www.sciencedirect.com
SCIENCE DIRECT®
Catalysis Today 87 (2003) 87–97
CATALYSIS TODAY
www.elsevier.com/locate/cattod

Photocatalytic performance of nanometer-sized Fe_xO_y/TiO_2 particle synthesized by hydrothermal method

Misook Kang [a,*], Suk-Jin Choung [a], Jong Yul Park [b]

[a] *Industrial Liaison Research Institute, Kyung Hee University, Yongin, Gyeonggi 449-701, South Korea*
[b] *Department of Chemistry, Busan National University, Jangjeundong 30, Kumjongku, Busan 609-735, South Korea*

Abstract

The nanometer particles of two Fe_xO_y/TiO_2's with high photocatalytic activities were obtained through hydrothermal treatment and impregnation method. The XRD result did not show the peaks assigned to the Fe components (for example Fe_2O_3, Fe_3O_4, FeO_3, and Fe metal) on the external surface of the anatase structure in the Fe_xO_y/TiO_2 attained through hydrothermal treatment. This meant that Fe components were well incorporated into the TiO_2 anatase structure. In addition, it exhibited uniform anatase structure with particle size of below 50 nm. The FeO_3 component on the external surface of the TiO_2 anatase structure was identified in the Fe-loaded TiO_2 prepared through the impregnation method. In particular, the FT-IR spectroscopy revealed that the Fe_xO_y/TiO_2 particle attained through hydrothermal treatment had higher hydrophilic property compared to the other catalysts. Together with the Fe component, they absorbed wavelength of above 370 nm. The band slightly shifted to the right without tail broadness, which was the UV absorption of Fe oxide in the Fe_xO_y/TiO_2 particle attained through hydrothermal method. This meant that Fe components were well inserted into the framework of the TiO_2 anatase structure. Despite the red shift in UV-Vis absorption, however, $CHCl_3$ decomposition on the Fe_xO_y/TiO_2 catalyst was not largely enhanced compared to pure TiO_2.
© 2003 Elsevier B.V. All rights reserved.

Keywords: Hydrothermal treatment; Impregnation method; Fe_xO_y/TiO_2; $CHCl_3$ decomposition

1. Introduction

Very recently, many works have been focusing on doping/mixing metals such as CdS, Fe_2O_3, Ga_2O_3, ZnO, Ag_2O, etc. [1–3] in TiO_2 anatase structures exhibiting lower band gap energies to activate photocatalysts using UV light with longer wavelengths. In particular, some studies [4–7] have introduced Fe into the anatase structure of TiO_2. These studies used a sol–gel method where titanium tetra-isopropoxide or $TiCl_4$ and Fe(III) acetyl acetone acted as precursors. The impregnation method providing Fe(III) precursors into anatase materials was investigated. Studies showed that Fe/Ti oxide photocatalysts prepared by sol–gel resulted in a much basic hydroxyl group than that obtained through the impregnation method. They showed that the surface of catalysts prepared by sol–gel was hydrophilic, which could be effective in decomposing volatile organic compounds even without noticeable increase in catalytic activity. This was attributed to the low dispersion of the added iron component on the external surface of the TiO_2. In addition, the amount of the incorporated Fe in the TiO_2 anatase structure was not very reliable. Consequently, properties of Fe/Ti oxide photocatalysts and their

* Corresponding author. Tel.: +82-31-201-2121; fax: +82-31-202-4765.
E-mail addresses: mskang@khu.ac.kr, msk1205@chollian.net (M. Kang).

0920-5861/$ – see front matter © 2003 Elsevier B.V. All rights reserved.
doi:10.1016/j.cattod.2003.09.011

performance under near visible light have yet to be fully clarified, although their absorption was known to have a tendency to shift to a longer wavelength.

Hydrothermal treatment was also introduced in this study. This method could be employed as an alternative to calcination in promoting crystallization under mild temperature. It has been widely applied to the synthesis of zeolites and ceramic powders containing various metal oxides [8,9]. It could also be used to control grain size, particle morphology, crystalline phase, and surface chemistry by regulating sol composition, reaction temperature, pressure, nature of solvent, additives, and aging time. In particular, the particles prepared through the hydrothermal method are expected to have larger surface area, smaller particle size, and higher stability than those obtained by other methods such as the sol–gel method [10,11]. Among the oxides reported so far, Fe/TiO_2 prepared through the hydrothermal method has yet to appear in available literature. Therefore, this study examined the Fe component of Fe_xO_y/TiO_2 incorporated into the TiO_2 anatase framework and synthesized through the hydrothermal method. The resulting characteristics were compared with samples prepared through the impregnation method.

2. Experimental

2.1. Catalyst preparation

The hydrothermal method for Fe_xO_y/TiO_2 catalysts is shown in Fig. 1. The impregnation method integrating Fe into the TiO_2 particle (prepared through the hydrothermal method) was also presented for comparison. Reagents used for the sol-mixture included titanium tetra-isopropoxide (TTIP) (99.95%, Junsei Chemical, Japan), and ferric nitrate ($Fe(NO_3)_2{\cdot}9H_2O$, Junsei Chemical, Japan) used as titanium and iron precursors. Isopropyl alcohol (Wako Pure Chem. Ltd.) was used as a solvent, with distilled water (mole ratio of H_2O/TTIP was 4:1) added for hydrolysis. As shown in Fig. 1, this study considered the hydrothermal method as a synthesis method. TTIP and iron precursors were mixed with organic solvent in an autoclave (model R-211, Reaction Engineering Inc., Korea) heated at 200 °C for 1 h at a rate of 5 °C/min. The weight percentage of the Fe:Ti precursor in gel mixtures was kept to 10.0:100.0. During thermal treatment, TTIP was hydrolyzed by the OH group in distilled water until Fe_xO_y/TiO_2 crystallization occurred. The resulting powder was washed with distilled water until pH 7 and then dried at 80 °C for 24 h.

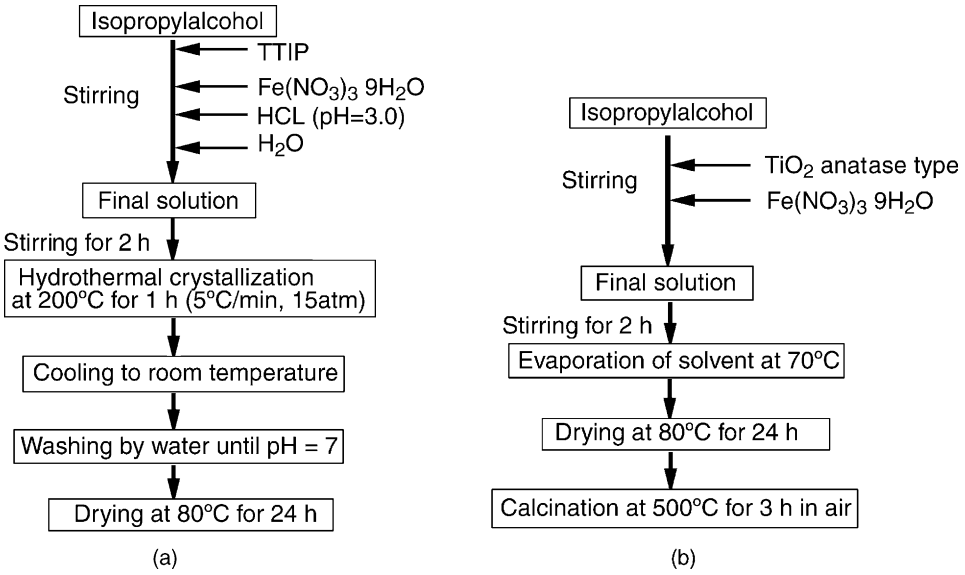

Fig. 1. Preparation of Fe_xO_y/TiO_2 powder by different methods: (a) hydrothermal method and (b) impregnation method.

On the other hand, during the impregnation method, used TiO_2 anatase particle was prepared through the hydrothermal method (60 m^2/g, 50–100 nm) then impregnated by 10.0 wt.% TTIP and H_2O solution. Finally, the sample was again calcined at 500 °C for 3 h to crystallize the Fe component.

2.2. Characterization of synthesized catalyst

Synthesized samples of Fe_xO_y/TiO_2 catalysts were identified through powder X-ray diffraction analysis (XRD, model PW 1830 from Philips) with nickel-filtered Cu Kα radiation (30 kV, 30 mA) at 2θ angle of 5–70°. The scan speed was 10°/min and the time constant 1 s. The particle size and shape of the Fe_xO_y/TiO_2 catalyst were observed through the scanning electron microscope (SEM, model JEOL-JSM35CF). Power was set to 15 kV. Chemical compositions were analyzed through ICP (inductively coupled plasma-AES model, Leeman Labs Inc., USA). Analysis was carried out with power set to 1 kW, pump rate to 1 ml/min, and coolant to 13 LPM/l min. Analyzed wavelengths of Fe and Ti were 259.94 and 334.94 nm, respectively. The BET surface area of the sample was measured through nitrogen gas adsorption with continuous flow method using chromatography equipped with a TCD detector at the liquid nitrogen temperature. A mixture of nitrogen and helium flowed as carrier gas from the GEMINI2375 model from Micrometrics. The sample was thermally treated at 300 °C for 1 h before nitrogen adsorption, with nitrogen gas pressure set to 10 atm. Particle size distribution of the samples was obtained through dynamic light scattering (DLS) spectrophotometer (BI 9000AT) after ultrasonic wave treatment using 140 W in water for 2 min. The zeta potential was measured to examine the stability and surface charge of the Fe_xO_y/TiO_2 photocatalysts prepared in this study. Its value was obtained using a Zetasizer 4000 at a 90° angle in distilled water. Before measurement, the sample was treated by ultrasonic waves using 100 W in water for 10 s. UV-Vis spectra were obtained using a Shimadzu MPS-2000 spectrometer equipped with a reflectance sphere. The special

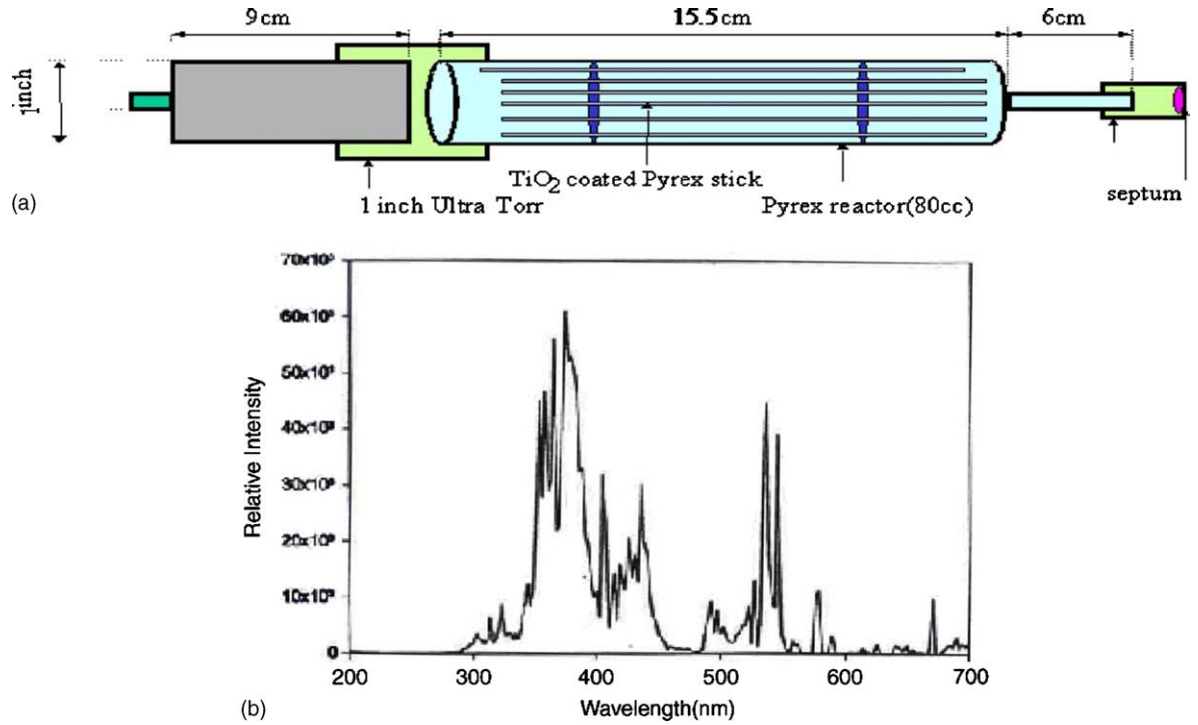

Fig. 2. Photoreaction system for $CHCl_3$ decomposition and wavelength of the UV lamp (365 nm): (a) reactor and (b) wavelength of UV lamp.

range was from 200 to 700 nm with $BaSO_4$ used as a reflectance standard. The photoluminescence spectroscopy measurement was also tested to examine the number of photo-excited electron hole pairs for all samples. Samples were measured at liquid nitrogen temperature (8 K) using He–Cd laser source of 325 nm. FT-IR spectra were recorded through a Mattson 1000 spectrometer using the diffused reflectance method. The powder sample mixed with KBr was pressed into pellet form. To diminish the influence of H_2O in the air, the pellet was kept at a temperature of 200 °C for 2 h in a dry oven prior to measurement. The scan range was from 400 to 3600 cm^{-1}, where 50 scans were accumulated to get 4 cm^{-1} resolution. Thermo-diagram was recorded on the TAS 100 Rigaku thermal analyzer system. The following were the experimental conditions: Rigaku, model TAS 100 as thermal analyzer; TGA range of 10 mg/FS; DSC range of 10 mcal/FS; heating rate of 5 K/min; Pt–Rh as thermocouple; α-Al_2O_3 as reference; chart speed of 1 mm/min; and argon environment.

2.3. Analysis of product for $CHCl_3$ decomposition in the photosystem

$CHCl_3$ decomposition was carried out using a flow reactor as shown in Fig. 2(a). For this experiment, 3 g catalysts were fixed on six Pyrex sticks 12 cm in length and 0.8 cm in diameter using 10 wt.% silane binder (from Enpion Inc., Korea). UV lamps (model BBL, 365 nm, 8W, 2×, 15 cm length × 1.5 cm diameter, Shinan Co., Korea) were used for photoreaction. The spectrum pattern is shown in Fig. 2(b). $CHCl_3$ concentration was fixed at 100 ppm, with the products in the photocatalytic decomposition analyzed using an FID-type gas chromatograph (GC). To determine exactly the products and intermediates, the GC was directly connected to the reactor of the $CHCl_3$ decomposition. The following are the conditions for GC:FID as detector; HP-640 column; injection temperature of 200 °C; initial temperature of 40 °C; final temperature of 200 °C; and detector temperature of 200 °C.

3. Results and discussion

3.1. Characterizations of photocatalysts

Fig. 3 shows the XRD patterns of Fe_xO_y/TiO_2 following hydrothermal and impregnation treatments. In general, the TiO_2 photocatalyst with anatase structure exhibited a higher performance for VOC decomposition than other types such as rutile, brookite, and amorphous. Based on this figure, the samples showed a well-developed anatase structure, although only ther-

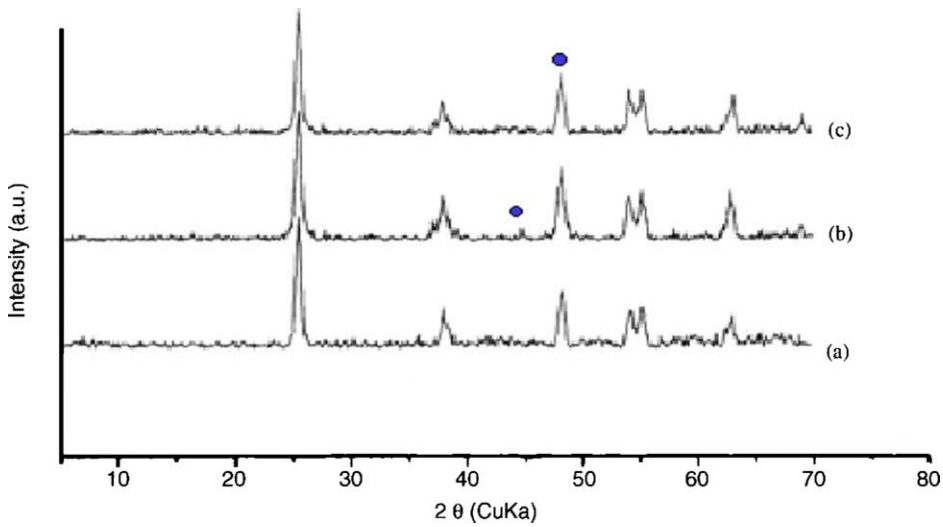

Fig. 3. XRD patterns of synthesized TiO_2 and Fe_xO_y/TiO_2: (a) TiO_2, (b) Fe_xO_y/TiO_2 prepared through the impregnation method, and (c) Fe_xO_y/TiO_2 synthesized through the hydrothermal method.

Table 1
Physical property of TiO_2 and Fe_xO_y/TiO_2 photocatalysts

Catalyst	Synthesis method	Composition in sol solution (wt.%)	Structure type	Composition in catalyst (atomic ratio)		Surface area (m^3/g)	Zeta potential (mV)
		TTIP:$Fe(NO_3)_3$		Ti:Fe	Fe/Ti		
Pure TiO_2	Hydrothermal method	–	Anatase	–	–	65.4	+24.0
Fe_xO_y/TiO_2	Hydrothermal method	100:10	Anatase	17.3:0.62	0.036	58.5	+41.5
Fe_xO_y/TiO_2	Impregnation method	100 (weight calculated in terms of TiO_2):10	Anatase	16.9:0.64	0.038	40.2	+38.5
Experimental method	–	–	XRD	ICP		BET	Zeta potential analyzer

mal treatment at 200 °C was done for 1 h. In general, 2θ values of Fe_2O_3, Fe_3O_4, FeO_3, and Fe metal are assigned around 33.3°, 36.0°, 46° and 49° (two closed circles), and 64°, respectively. Peaks assigned to the Fe component were not observed in the XRD pattern of Fe_xO_y/TiO_2 synthesized through hydrothermal treatment. This result may be attributed to the fact that Fe component was well substituted into the Ti site. In the case of Fe-loaded sample prepared through the impregnation method, one peak assigned to FeO_3 [Fe(VI)] at 46° (closed circle) was observed after calcination at 500 °C for 1 h. This result confirmed that the hydrothermal method was very useful in dispersing Fe component to Ti sites in TiO_2 anatase structure. On the other hand, the width of the peak was slightly broader in Fe_xO_y/TiO_2 compared with that of the pure TiO_2 particle. In general, the width of the XRD peak corresponded to the crystallite sizes of porous materials. Given a broad width, the crystallites had smaller size. In particular, crystallites were smaller in the sample including transition metals such as Ni and Fe [12].

Physical properties for these catalysts are given in Table 1. In the ICP result, the amount of Fe incorporated into the catalyst was higher in Fe_xO_y/TiO_2 attained through the impregnation method than that synthesized through the hydrothermal method. Although the BET surface areas of Fe_xO_y/TiO_2 catalysts were found to be smaller than that of pure TiO_2, they still exceeded 58 m^2/g in the sample synthesized through the hydrothermal method and registered 40 m^2/g in the sample attained through the impregnation method. Since the surface areas of Fe_xO_y/TiO_2 were smaller than that of pure TiO_2 after the incorporation of Fe, because that the surface of TiO_2 was expected to be partially covered by the Fe component. These aforementioned results confirmed that the hydrothermal method was more efficient in preparing Fe_xO_y/TiO_2 compared with the impregnation

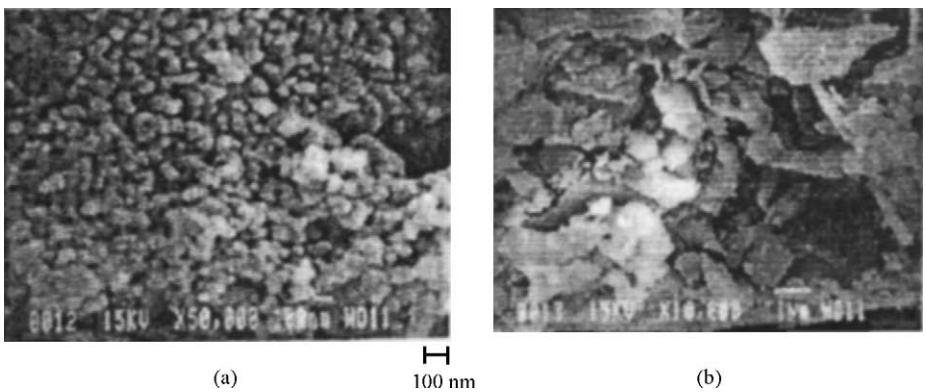

Fig. 4. SEM photographs of synthesized Fe_xO_y/TiO_2: (a) Fe_xO_y/TiO_2 synthesized through the hydrothermal method and (b) Fe_xO_y/TiO_2 prepared through the impregnation.

method. The zeta potential was also found to be highest in Fe_xO_y/TiO_2 attained through the hydrothermal method, although those of all the catalysts were positive. Since the zeta potential value is generally proportional to the crystal surface stability and used as an index for stability, it can be concluded that the surface of Fe_xO_y/TiO_2 attained through the hydrothermal method is more stable than the other samples.

The SEM photographs of samples are shown in Fig. 4. Used pure TiO_2 sample attained through the impregnation method showed relatively uniform and spherical particles with a size of about 50 nm. Fe_xO_y/TiO_2 (a) synthesized through the hydrothermal method was about 50 nm. Fe_xO_y/TiO_2 (b) attained through the impregnation method had coagulated particles of more than 100 nm.

To assign a reliable particle size distribution, differential light scattering (DLS) test was done and the result presented in Fig. 5. Pure TiO_2 particles were sharply distributed around 30–45 nm. On the other hand, the Fe-loading TiO_2 was largely distributed around 30–90 nm. The size distribution showed a regular form of around 25–40 nm in Fe-incorporated TiO_2 attained through the hydrothermal method. In general, the particle sizes of micro-porous materials decreased with the addition of some transition metals. Therefore, this result may be attributed to the presence of Fe component in the TiO_2 framework [12].

FT-IR spectra are shown in Fig. 6. The band around 1200 cm^{-1} assigned to the Ti–O–Ti bending was observed [13]. The band in Fe_xO_y/TiO_2 was weaker, shifting more toward the longer wavelength than that in pure TiO_2. This result meant that the Ti–O–Ti bending mode and the interaction between Ti and O decreased because of Fe substitution. Unlike the pure TiO that is not found in the 3700 cm^{-1} band assigned to the OH stretching band, Fe_xO_y/TiO_2's synthesized through the hydrothermal method exhibited more hydrophilic behavior compared with pure TiO_2.

To confirm the effect of added iron on the titanium dioxide anatase framework, the NH_3-TPD test was performed and profiles shown in Fig. 7. These profiles consisted of two peaks: one appeared at a low temperature range of 100–150 °C and the other at a high temperature range of 350–400 °C. The low and high temperature peaks corresponded to the weak and strong acid sites, respectively. In case of pure TiO_2 and Fe_xO_y/TiO_2 prepared through the impregnation method, only the peak assigned to weak acid sites or H_2O desorption was found while the second peak around 400 °C was present in the Fe_xO_y/TiO_2 sample synthesized through the hydrothermal method. This result explained the new acid sites on the TiO_2 photocatalyst framework generated by the addition of Fe component. Therefore, the OH group affecting VOC photocatalytic removal generated by these acid sites was confirmed.

The amount of water adsorbed in photocatalysts is compared in Table 2. It increased more in the case of Fe_xO_y/TiO_2 synthesized through the hydrothermal method than the other catalysts. Ozawa presented a useful equation to calculate the activation energy of various thermal reactions, based on the shifts of the maximum deflection temperature T_m of DSC

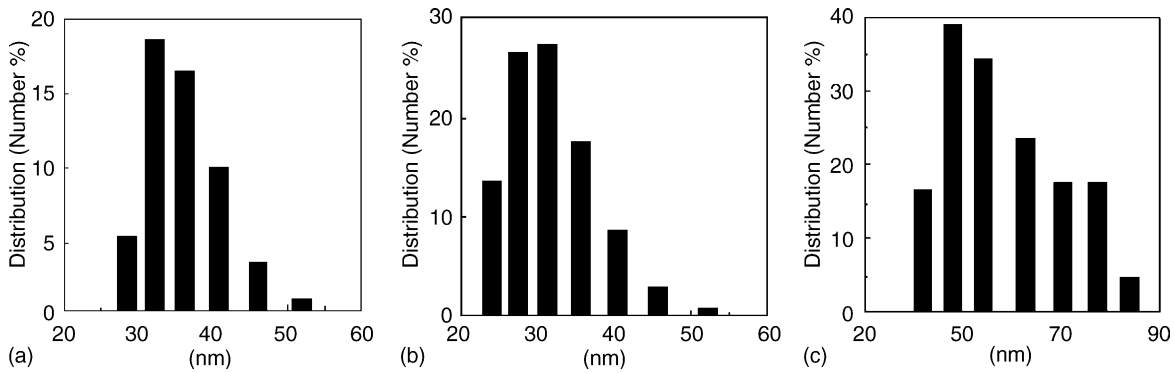

Fig. 5. Particle distribution of synthesized TiO_2 and Fe_xO_y/TiO_2: (a) TiO_2, (b) Fe_xO_y/TiO_2 synthesized through the hydrothermal method, and (c) Fe_xO_y/TiO_2 prepared through the impregnation method.

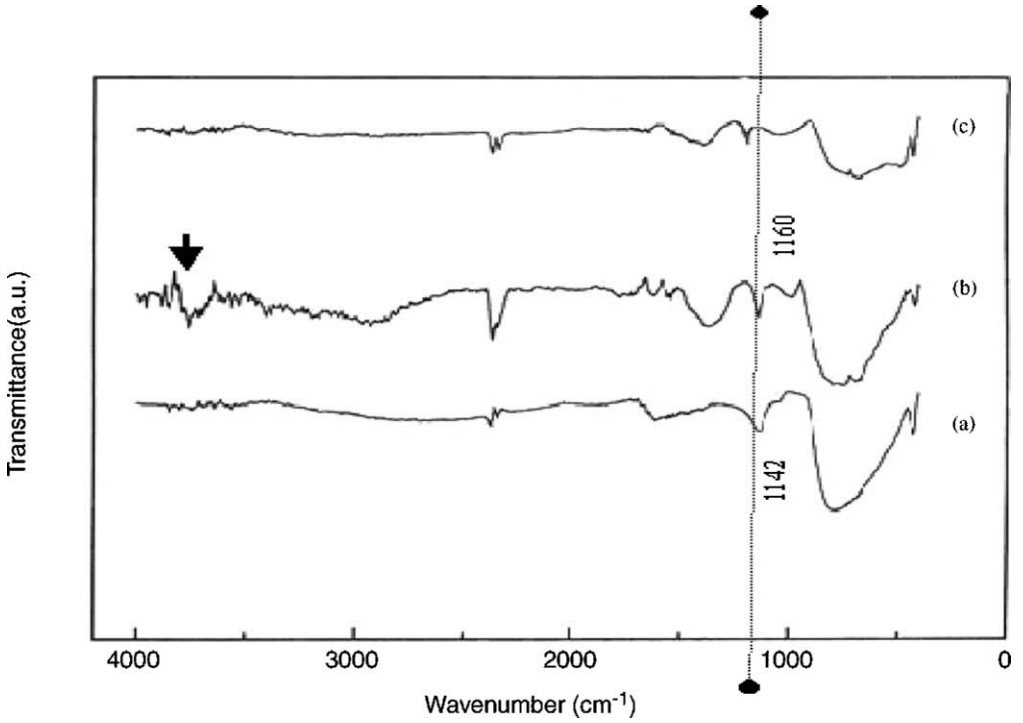

Fig. 6. FT-IR spectra of synthesized TiO_2 and Fe_xO_y/TiO_2: (a) TiO_2, (b) Fe_xO_y/TiO_2 synthesized through the hydrothermal method, and (c) Fe_xO_y/TiO_2 prepared through the impregnation method.

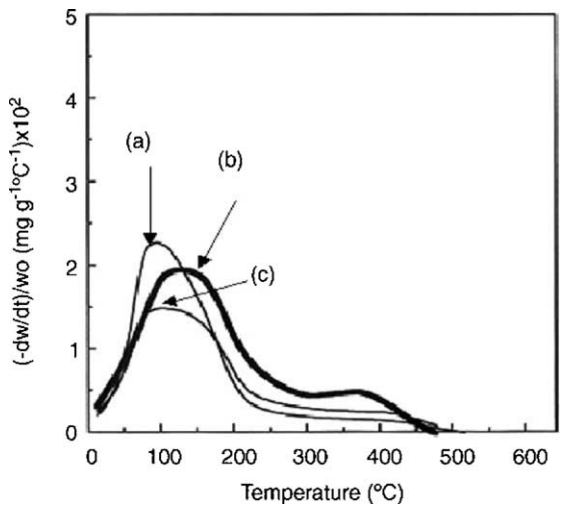

Fig. 7. NH_3-TPD curves of synthesized TiO_2 and Fe_xO_y/TiO_2: (a) TiO_2, (b) Fe_xO_y/TiO_2 synthesized through the hydrothermal method, and (c) Fe_xO_y/TiO_2 prepared through the impregnation method.

thermograms given the changes in heating rates:

$$\log\phi + \frac{0.4567E}{RT_m} = \text{constant}$$

Here ϕ is the heating rate, T_m the maximum deflection temperature, E the activation energy, and R the constant gas.

The activation energy can be derived from the slope $0.4567E/R$ from the plot of $\log\phi$ versus $1/T_m$. This

Table 2
Desorption amounts of H_2O pre-absorbed on photocatalysts and activation energy on TiO_2 and Fe_xO_y/TiO_2 photocatalysts

Catalyst	Desorption amounts of H_2O (mmol)	Activation energy (kcal/mol)
Pure TiO_2	0.0062	14.40
Fe_xO_y/TiO_2 by hydrothermal method	0.0169	15.70
Fe_xO_y/TiO_2 by impregnation method	0.0027	8.90

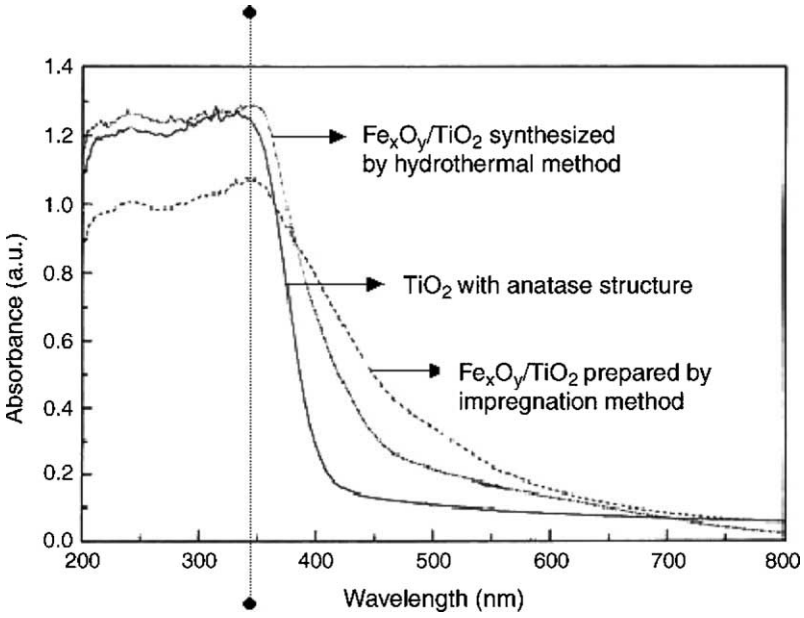

Fig. 8. UV-Vis spectra of synthesized TiO_2 and Fe_xO_y/TiO_2.

experiment is often used to discuss the hydrophilic property of a structure. This method was used by this present study to determine the activation energy for dehydration. In the case of Fe_xO_y/TiO_2 synthesized through the hydrothermal method, the activation energy needed to break the bond formed between H_2O molecule and anatase framework increased. This result meant that Fe_xO_y/TiO_2 synthesized through the hydrothermal method was more hydrophilic than the other catalysts.

Fig. 8 shows the UV-Vis spectra. In general, the absorption of Fe^{3+} in octahedral symmetry is known to appear above 430, 475, and 520 nm [11] while the absorption of Ti^{4+} tetrahedral symmetry appears around 370 nm. In the case of Fe_xO_y/TiO_2 prepared through the impregnation method, almost all bands assigned to the Fe ion octahedral symmetry were broadly shown as long tails. This meant that the Fe component was physically connected to the external surface of the TiO_2 anatase structure. On the other hand, in the sample attained through the hydrothermal method, the band slightly shifted to the right without tail broadness. This meant that the Fe component was well inserted into the framework of the TiO_2 anatase structure.

Fig. 9 shows the photoluminescence emission value measured through the photoluminescence spectra. Generally, when semiconducting material receives energy from the outside, the electron from the valence band transfers to the conduction band and strongly oxidizes some volatile organic compounds. Nonetheless, some photo-excited electrons are trapped in shallow or deep traps and slowly recombine with holes in the conduction band. This recombination process has radiation and nonradiation recombination. The former can be detected through photoluminescence spectroscopy. Consequently, when the photoluminescence emission value is high, the number of recombination electrons should decrease and the photoactivity of the material for decomposing volatile organic compounds should increase. As shown in this figure, the band is present only in one type. Compared with pure TiO_2, the band shifted to the right of the Fe_xO_y/TiO_2, and the value was almost the same as that of the base line regulation. At this point, the band shift meant the decrease of sub-band gap or deep traps. The influence of the shift to the right on photocatalytic performance was not clearly determined, however.

3.2. Photodecomposition of $CHCl_3$ on Fe_xO_y/TiO_2

Photocatalytic oxidation of organic compounds attracts considerable interest due to its versatile

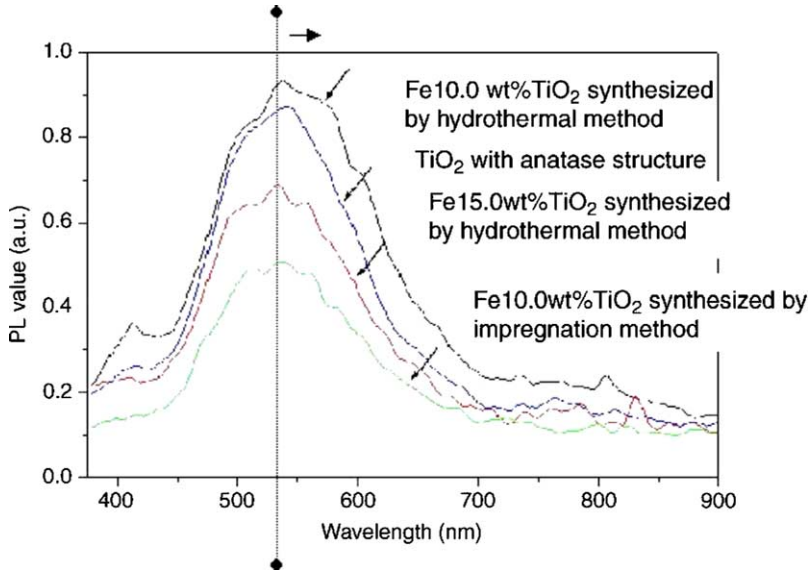

Fig. 9. PL (photoluminescence) spectroscopy of synthesized Fe_xO_y/TiO_2.

environmental applications or control and eventual destruction of hazardous wastes. In particular, some specific compounds that are of interest include compounds containing chloride ion such as 4-chlorophenol, pentachlorophenol, trichloroethylene (TCE), perchloroethylene (PCE), CCl_4, $HCCl_3$, CH_2Cl_2, vinyl chloride, and *p*-chlorobenzene. This study selected $CHCl_3$ to determine the photocatalytic performance of Fe_xO_y/TiO_2.

Fig. 10(A) shows the performance of $CHCl_3$ decomposition on Fe_xO_y/TiO_2 photocatalyst under UV light of 365 nm. $CHCl_3$ decomposition on pure TiO_2

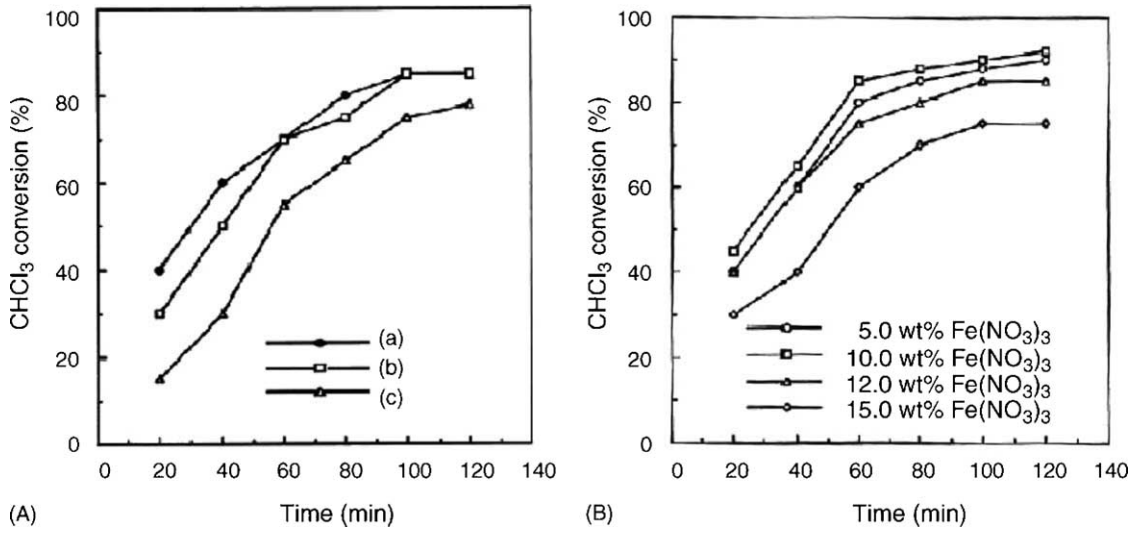

Fig. 10. $CHCl_3$ conversions with reaction time of TiO_2 and Fe_xO_y/TiO_2 catalysts: (A) on various catalysts and (B) on Fe_xO_y/TiO_2 synthesized through the hydrothermal method. (a) TiO_2 and (b) Fe_xO_y/TiO_2 synthesized through the hydrothermal method, and (c) Fe_xO_y/TiO_2 prepared through the impregnation method. Reaction conditions: $CHCl_3$ concentration of 100 ppm, catalyst weight of 3.0 g, UV-light intensity of 365 nm with 24 W/m^2, and batch reaction system.

photocatalyst was less than 90% after 120 min. In the case of Fe_xO_y/TiO_2, the final conversion of Fe-incorporated TiO_2 was almost the same as that of pure TiO_2. The decomposition decreased on Fe-loading TiO_2, however. On the other hand, Fig. 10(B) shows the effect of the Fe component on $CHCl_3$ decomposition on Fe-incorporated TiO_2 photocatalyst. It showed that $CHCl_3$ decomposition was enhanced by up to 10 wt.% of Fe concentration but decreased with an increase in the Fe component. This result could be attributed to the increase of Fe_2O_3 or FeO_3 components on the external TiO_2 framework that partially covered the TiO_2 surface.

On the other hand, $CHCl_3$ decompositions of TiO_2 and Fe_xO_y/TiO_2 were also done in a continuous photosystem shown in Fig. 11. Both TiO_2 and Fe_xO_y/TiO_2 were synthesized through the hydrothermal method, with $CHCl_3$ conversions about 60% after 10 h. The $CHCl_3$ conversion was about 30% on Fe_xO_y/TiO_2 prepared through the impregnation method. These results showed that $CHCl_3$ decomposition on the Fe_xO_y/TiO_2 catalyst was not largely enhanced compared with pure TiO_2, despite the red shift in UV-Vis absorbance.

These results are presented in a model shown in Scheme 1. The TiO_2 band gap may be small as a result of the red shift in UV-Vis absorbance through the addition of the Fe component. The simultaneous

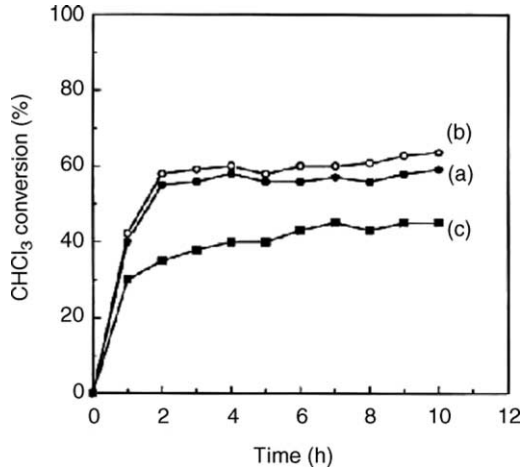

Fig. 11. $CHCl_3$ conversions on photocatalysts in a continuous system: (a) TiO_2, (b) Fe_xO_y/TiO_2 synthesized by hydrothermal method, and (c) Fe_xO_y/TiO_2 prepared by impregnation method. Reaction conditions: $CHCl_3$ concentration of 100 ppm, catalyst weight of 3.0 g, UV-light intensity of 365 nm with 24 W/m^2, O_2 gas of 150 ml, and continuous reaction system.

recombination time between the electron and the hole that affected photocatalytic performance was shown in Scheme 1. The addition of the Fe component (the shorter band gap energy) did not significantly affect photocatalytic performance. Nonetheless, the

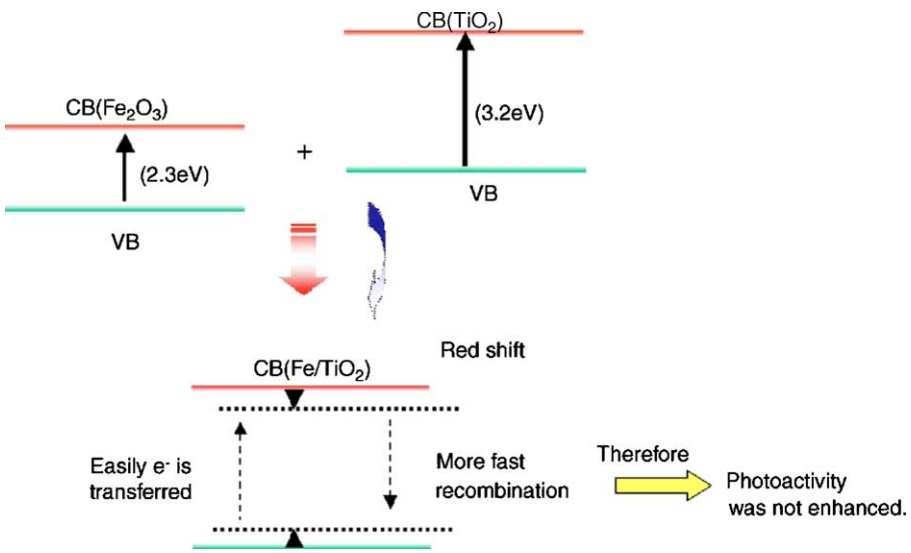

Scheme 1. A possible model of Fe_xO_y/TiO_2 from results of the UV-Vis spectra and photocatalytic performance.

conversion of $CHCl_3$ on Fe_xO_y/TiO_2 synthesized through hydrothermal treatment was slightly higher than that on Fe-loading TiO_2 particle prepared through the impregnation method.

4. Conclusion

The nanometer particle Fe_xO_y/TiO_2 with high photocatalytic activity was successfully obtained through hydrothermal treatment. The following were the main results:

1. The Fe component was well incorporated into the TiO_2 anatase structure during hydrothermal treatment.
2. Fe-incorporated TiO_2 catalyst exhibited uniform anatase structure with particle size below 50 nm after synthesis at 200 °C for 4 h in isopropyl alcohol without any treatment.
3. FT-IR spectroscopy and DSC analysis confirmed that the Fe_xO_y/TiO_2 particle attained through the hydrothermal treatment had higher hydrophilic property than the other catalysts.
4. Despite the red shift in UV-Vis absorbance, $CHCl_3$ decomposition on the Fe_xO_y/TiO_2 catalyst was not largely enhanced compared with pure TiO_2.
5. The conversion of $CHCl_3$ was slightly higher on Fe_xO_y/TiO_2 synthesized through hydrothermal treatment than Fe-loading TiO_2 particle prepared through the impregnation method.

Consequently, it was confirmed that transition metal could be well incorporated into the anatase structural framework through the hydrothermal method, later inducing a decrease in the band gap of semiconducting material not largely affected by photoactivity.

Acknowledgements

This work was supported by the Korea Research Foundation (KRF-2001-E20007). The authors are grateful for its financial support.

References

[1] G. Dagan, S. Sampath, O. Lev, Chem. Mater. 7 (1995) 446.
[2] T. Takata, Y. Furumi, K. Shinohara, A. Tanaka, M. Hara, J.N. Kondo, K. Domen, Chem. Mater. 9 (1997) 501.
[3] M.K. Arora, N. Sahu, S.N. Upadhyay, A.S.K. Sinha, Ing. Eng. Chem. Res. 38 (1999) 2659.
[4] H. Kim, N. Hara, K. Sugimoto, J. Electrochem. Soc. 146 (1999) 955.
[5] S.H. Ehrman, S.K. Friedlandar, M.R. Zachariah, J. Mater. Res. 14 (1999) 4551.
[6] F. Chen, J. Zhao, Catal. Lett. 58 (1999) 254.
[7] F. Boccuzzi, A. Chiorino, M. Manzoli, D. Andreeva, T. Tabakova, J. Catal. 188 (1999) 176.
[8] B.B. Lakshmi, P.K. Dorhout, C.R. Martin, Chem. Mater. 9 (1997) 857.
[9] M. Kang, M.-H. Um, J.-Y. Park, J. Mol. Catal. 150 (1999) 195.
[10] M. Kang, S.-Y. Lee, C.-H. Chung, S.M. Cho, G.Y. Han, B.-W. Kim, K.J. Yoon, J. Photochem. Photobiol. A 144 (2001) 185.
[11] S.-H. Lee, M. Kang, S.M. Cho, G.Y. Han, B.-W. Kim, K.J. Yoon, C.-H. Chung, J. Photochem. Photobiol. A 146 (2001) 121.
[12] M. Kang, T. Inui, Catal. Lett. 53 (1999) 171.
[13] J. Arana, O. Gonzalez Diaz, J.M. Dona Rodriguez, J.A. Herrera Melian, C. Garriga, I. Cabo, J. Perez Pena, M. Carmen Hidalgo, J.A. Navio-Santos, J. Mol. Catal. A, in press.